Cross sections for electron-impact excitation of Krypton

J. Ethan Chilton,* M. D. Stewart, Jr., and Chun C. Lin
Department of Physics, University of Wisconsin, Madison, Wisconsin 53706
(Received 8 March 2000; published 17 August 2000)

Electron-impact excitation cross sections for Kr have been measured by means of the optical method over a range of incident-electron energies between onset and 250 eV. By measuring cascade transitions into the $4p^5 5p$ levels from higher-lying levels and subtracting this contribution from the observed transitions out of the $4p^5 5p$ levels, we are able to determine the cross sections for direct electron excitation into the ten levels of the $4p^5 5p$ configuration ($2p$ in Paschen's notation). The general trends of these cross sections for Kr are compared with previous measurements from our labs on Ne, Ar, and Xe. We note that the optical emission cross sections for transitions from levels resonant with the ground level vary with gas pressure. Fitting this observed pressure dependence to a simple model allows us to test theoretical values of the transition coefficients for these levels.

PACS number(s): 34.80.Dp, 34.80.My

I. INTRODUCTION

Electron excitation processes of the rare gases are of great importance from the standpoint of understanding basic electron-atom interactions and have applications to various fields such as atmospheric science, lighting technology, gas lasers, and plasma processing. The recent surge of interest in these areas has stimulated a large body of studies of the electron-impact excitation cross sections. In spite of the similarity in electronic structure of the four rare gases (neon through xenon), Kr and Xe differ from Ne and Ar in one aspect that has a strong influence on electron-impact excitation. Consider, for instance, the $3p^5 4p$ configuration of argon, which consists of ten levels with the total angular momentum J ranging from 0 to 3. The energy separations of these levels are governed by the coupling between the orbital and spin angular momenta of the $3p^5$ core and the $4p$ electron. The magnitudes of the interactions of the four angular momentum vectors are such that their coupling does not conform closely to standard vector coupling schemes such as the *LS*, *jj*, or *jK* coupling, and is described instead by the intermediate coupling. The ten levels are more or less evenly spread out over a range of 0.6 eV, which is small compared to the ionization energy (2.6 eV), as shown in Fig. 1. The same trend is seen in neon, in which the ten levels of the $2p^5 3p$ configuration also range within 0.6 eV of one another. The situation is, however, very different for the corresponding configuration of xenon, $5p^5 6p$. Here the spin-orbit coupling of the $5p^5$ core is much stronger than the coupling of the $5p^5$ core with the $6p$ electron. To construct the term levels within this configuration, we start with the spin-orbit interaction of the core, which yields the $5p^5(^2P_{3/2})$ and $5p^5(^2P_{1/2})$ pair with a spacing of 1.3 eV. The lower member $^2P_{3/2}$ then couples with the orbital and spin angular momenta of the $6p$ electron, resulting in six levels whose spacings are much smaller than the $5p^5$ core $^2P_{3/2}$-$^2P_{1/2}$ splitting. Coupling of the upper member $^2P_{1/2}$ with the $6p$ electron likewise generates four closely spaced levels. Figure 1 shows the $5p^5 6p$ configuration consisting of a lower subset of six levels and an upper subset of four. The ionization energy of the upper group is about 1.1 eV, which is less than one-half of the ionization energy of the lower group ($\sim$2.4 eV). This is in contrast to the case of argon in which all ten levels of the $3p^5 4p$ configuration have nearly the same ionization energy. Because of the dominance of the spin-orbit coupling of the $5p^5$ core, all the excited configurations $5p^5 nl$ of xenon exhibit the same two-group structure associated with the $^2P_{3/2}$ and $^2P_{1/2}$ members of the core.

The difference in the grouping of energy levels between argon and xenon is reflected in the electron-impact excitation cross sections. For argon (and neon) the cross sections of a level within a given configuration are related to the parity of the total angular momentum J of that level. Stated more generally, the levels in the $3p^5 nl$ configuration with odd values of $J+l$ tend to have larger cross sections than those with even $J+l$ [1–4]. The pattern of variation, however, is different for xenon. Here, the lower subgroup of the $5p^5 6p$ levels have distinctly larger cross sections than the upper subgroup, although within each subgroup the even-J levels do have larger cross sections than the odd-J levels [5]. As suggested

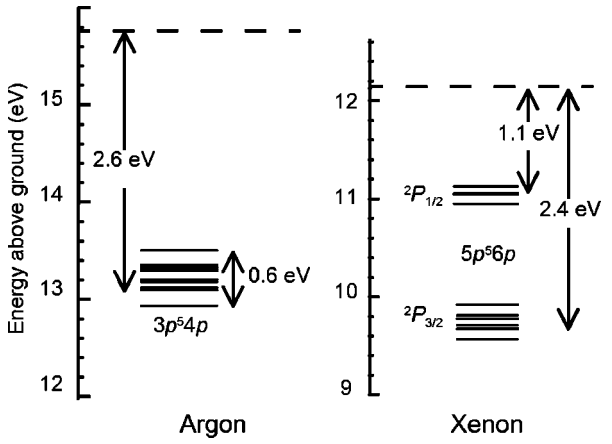

FIG. 1. Lowest-lying p manifolds in argon and xenon in relation to the ionization limit (dashed horizontal lines).

*Present address: Center for Naval Analyses, Alexandria, VA 22302.

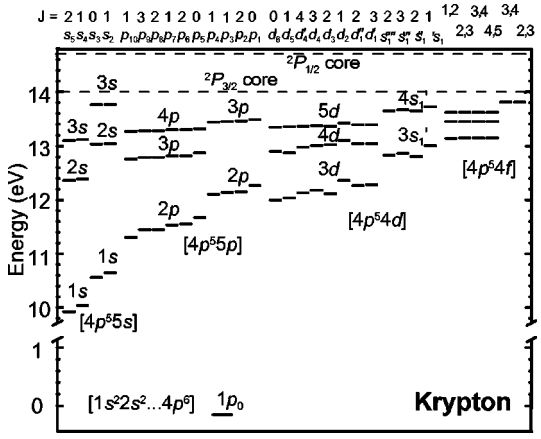

FIG. 2. Partial energy level diagram for krypton. Configuration notation is provided in brackets below each manifold of excited levels. Paschen's notation is given above each manifold, with the designation for each level listed at the top of the figure, along with the J values. The dashed lines represent the ionization limits for the two core configurations.

in Ref. [5], the reason for the large difference in excitation cross sections between the two subgroups is that the energy levels in the upper subgroup have much smaller ionization energy. Therefore, they have more diffuse wave functions than the levels in the lower subgroup, making excitation from the ground state (with a compact wave function) into the upper subgroup less favorable. In contrast to xenon, the energy levels of argon in the $3p^5 4p$ configuration (also the $2p^5 3p$ of neon) all have nearly the same ionization energy. Neither the energy levels nor the excitation cross sections exhibit the pattern of two subgroups.

Figure 2 shows the energy levels of krypton, which have a pattern intermediate between xenon and argon. The ten levels in the $4p^5 5p$ configuration ($2p$ in Paschen's notation) still segregate into two subgroups associated with the $^2P_{3/2}$ (lower) and $^2P_{1/2}$ (upper) doublet of the $4p^5$ core, but the doublet separation (0.7 eV) is not much larger than the energy span of the lower subgroup ($\sim$0.4 eV). The average ionization energy of the lower subgroup is only about 40% higher than that of the upper subgroup as opposed to the factor-of-2 difference in xenon. However, no studies of the systematics of the cross sections for the Kr ($4p^5 5p$) levels, to our knowledge, have been reported in the literature. In this paper we measure the excitation cross sections for the $4p^5 5p$, $4p^5 ns$, and $4p^5 nd$ levels and compare the results with those of neon, argon, and xenon.

Another important aspect of the electron excitation processes is the pressure dependence. Previous studies of the other rare gases have revealed that the optical emission cross sections for most of the transitions increase with increasing target gas pressure [1,2,4,5]. The degree of dependence is strongest for xenon and weakest for neon. A full understanding of this pressure dependence is essential in determining the excitation cross sections of Kr from the optical measurements.

Krypton plays an important role in laser, plasma, and lighting technology. Analysis of the operation of KBr lasers requires a detailed knowledge of electron excitation of the krypton atoms [6]. Another area of application is plasma diagnostics, where the electron temperature and species concentration of a plasma may be determined from measurements of the intensities of emissions from excited rare-gas atoms in the plasma [7]. This actinometry method requires accurate values of the electron excitation cross sections [8]. The use of Kr gas in electrodeless discharge lamps also underscores the need for a detailed knowledge of the electron excitation processes in krypton [9].

II. EXPERIMENTAL METHOD

Excitation into a particular energy level was detected by observing photons emitted as the excited krypton atom decayed out of the level of interest to lower levels. This procedure, known as the optical method, is described in more extensive detail elsewhere [10], and is reviewed only briefly here. By measuring the number of photons per unit time per electron beam length emitted as the excited atoms undergo transitions from level i to level j, Φ_{ij}, the optical emission cross section Q_{ij} is defined as

$$Q_{ij}^{\mathrm{opt}} = \frac{\Phi_{ij}}{n_0 (I/e)}, \tag{1}$$

where I represents the electron beam current, e the charge of an electron, and n_0 the number density of atoms. Summation of the cross sections for all transitions into a level i from higher levels k is termed the *cascade cross section*. Similarly, the sum of cross sections for all transitions out of i into lower levels j is termed the *apparent cross section*:

$$Q_i^{\mathrm{casc}} = \sum_{k>i} Q_{ki}^{\mathrm{opt}}, \quad Q_i^{\mathrm{app}} = \sum_{j<i} Q_{ij}^{\mathrm{opt}}. \tag{2}$$

The difference between apparent and cascade cross sections yields the direct cross section for electron-impact excitation into level i:

$$Q_i^{\mathrm{dir}} = Q_i^{\mathrm{app}} - Q_i^{\mathrm{casc}}. \tag{3}$$

Cascade radiation into the $4p^5 5p$ levels originates primarily from the $4p^5 6s$, $4p^5 7s$, $4p^5 4d$, and $4p^5 5d$ levels. Most of these transitions lie in the infrared portion of the spectrum, and so until now have not been studied. Recent advances in the use of the Fourier-transform spectrometer (FTS) have made possible the detection of infrared radiation in weak-emission electron excitation experiments [1]. This technique has allowed us to examine infrared transitions in He [11], Ne [4], Ar [1,2], and Xe [5]. The experimental methods used to study krypton are identical to those described previously. We present only a brief description here.

The experiment consists of a static gas target contained within a vacuum chamber. An electron gun capable of producing a $\sim$100 μA beam between 5 and 250 eV is located within the chamber. Emissions from atoms excited by the electron beam pass through a CaF_2 window in the chamber and are directed to the entrance slit of a Fourier-transform spectrometer (Nicolet model MagnaIR-860). By choosing

appropriate beam splitter/detector combinations, the spectrum from 0.3 to 6.0 μm can be investigated. Emissions in the wavelength range between 0.3 and 0.9 μm are detected by a photomultiplier tube (PMT) with quartz beam splitter. Longer wavelengths are detected with InGaAs and InSb detectors and a KBr beam splitter. The FTS provides relative values for the optical emission cross sections. These are placed on an absolute scale by a bridging calibration using a monochromator/PMT detector system with an identical collision chamber, as described in Ref. [10]. This monochromator/PMT system can also be used for measuring smaller optical cross sections for emission in the 300–900 nm range.

III. RESULTS AND DISCUSSION

Our principal interest in this paper is the excitation of the ten levels in the $4p^5 5p$ configuration. This entails the measurement of the optical cross sections for the $4p^5 5p \rightarrow 4p^5 5s$ emission lines, in order to determine the apparent excitation cross sections, and the cross sections for transitions into the $4p^5 5p$ levels from higher levels to determine the cascades. Because of the two-subgroup pattern of the energy levels, the upper subgroup of $4p^5 5p$ levels lie partially above the lower subgroup of $4p^5 4d$ (see Fig. 2). This provides additional decay channels for some of the $4p^5 5p$ levels. However, transitions from the upper subgroup of $4p^5 5p$ into the lower subgroup of $4p^5 4d$ entail a change of the $4p^5$ core ($^2P_{1/2}$ to $^2P_{3/2}$). The frequencies of the radiation emitted in such transitions are much lower than those from same-core transitions; hence, the transition rates are expected to be exceedingly low. Using the theoretical transition probabilities calculated by Aymar and Coulombe [12], we estimate the branching fractions of these transitions to be less than 0.007%, which can be safely neglected.

We have determined the cascade into the $4p^5 5p$ levels by measuring the optical cross sections for the $4p^5 ns \rightarrow 4p^5 5p$ ($n=6,7,8$) and $4p^5 nd \rightarrow 4p^5 5p$ ($n=4,5,6$) emissions. Subtracting the total cascade from the apparent excitation cross sections gives the direct excitation cross sections for the $4p^5 5p$ levels. Our measurements of the $4p^5 ns \rightarrow 4p^5 5p$ and $4p^5 nd \rightarrow 4p^5 5p$ cascade emissions also yield the apparent excitation cross sections for a number of $4p^5 ns$ and $4p^5 nd$ levels. Although we are not able to detect the cascade radiation into the $4p^5 ns$ and $4p^5 nd$ levels in order to determine their *direct* excitation cross sections, the *apparent* excitation results, as we will see, reveal some interesting features of the cross section data.

In this section, we first discuss the pressure dependence of the optical emission cross sections and its relation to reabsorption of resonant radiation. This will be followed by the measurements of the $4p^5 ns \rightarrow 4p^5 5p$ and $4p^5 nd \rightarrow 4p^5 5p$ cascades and discussions of the apparent excitation cross sections of the $4p^5 ns$ and $4p^5 nd$ levels in Secs. III B and III C. Determination of the direct excitation cross sections of the $4p^5 5p$ levels will be presented in Sec. III D. We discuss in Secs. III E and III F the general trends of the cross sections of the ten $4p^5 5p$ levels and their relations to the corresponding results of the other rare gases. Finally, we compare our cross section results with previous experiments and theory.

A. Pressure effects

The optical emission cross sections of the rare gases are known to increase with pressure even at 1 mTorr or less. Recent studies of Ar, Xe, and Ne have traced the origin of this pressure effect to resonance radiation trapping through reabsorption. Consider electron excitation into a resonant level α, which radiatively decays to the ground level (0) as well as to a nonresonant level β. The resonant photon emitted by the $\alpha \rightarrow 0$ transition may be reabsorbed by a nearby ground-level atom, exciting it to α. This gives another chance for an $\alpha \rightarrow \beta$ transition to occur. As the pressure increases, it becomes more likely that resonant photons will be reabsorbed in the gas. The effect is to increase the branching fraction of the $\alpha \rightarrow \beta$ channel at the expense of the $\alpha \rightarrow 0$ channel. The optical cross section for the $\alpha \rightarrow \beta$ emission therefore increases with pressure and reaches a high-pressure asymptotic limit corresponding to complete reabsorption of the resonant photons.

A quantitative analysis of the effects of resonance radiation reabsorption on the pressure dependence of the $\alpha \rightarrow \beta$ emission cross section has been offered by Gabriel and Heddle [13]. The key quantity of their model is the fraction of resonant photons escaping the collision chamber, which is a function of the gas pressure and is denoted by $g(P)$. This function has been examined in some detail [14] and can be recast from a function of pressure for a particular gas to a universal form for all gases by writing it as a function of the dimensionless quantity $k_0\rho$, where ρ is a characteristic collision radius for the experimental geometry and k_0 is the absorption coefficient of the resonant line, and is linear in P. The optical excitation cross section for the $\alpha \rightarrow \beta$ transition at a pressure P is then given by [13]

$$Q_{\alpha\beta}^{\mathrm{opt}}(P) = A_{\alpha\beta} \frac{Q_\alpha^{\mathrm{dir}} + Q_\alpha^{\mathrm{casc}}}{A'_\alpha + A_{\alpha 0} g(k_0\rho)}, \tag{4}$$

where $A_{\alpha\beta}$ and $A_{\alpha 0}$ are the $\alpha \rightarrow \beta$ and $\alpha \rightarrow 0$ transition probabilities, respectively, and A'_α is the sum of the transition probabilities for all transitions from α into the lower levels except the ground level. These transition probabilities are calculated in the absence of pressure effects, so that $g(k_0\rho)$ contains the only pressure dependence in the right-hand side of Eq. (4), when the pressure dependence of Q_α^{casc} is neglected as was done in Ref. [4]. In this paper we are mainly interested in the optical cross sections for two types of transitions: (a) transitions into the $4p^5 5p$ levels from the higher levels, and (b) transitions from the $4p^5 5p$ levels into the lower levels. Since the $4p^5 5p$ levels are not optically connected to the ground level, type (a) includes transitions from resonant levels such as $4p^5 ns(J=1) \rightarrow 4p^5 5p$ and $4p^5 nd(J=1) \rightarrow 4p^5 5p$, which can be analyzed by using Eq. (4). On the other hand, Eq. (4) is not applicable to type (b). The effect of pressure on the apparent excitation cross sections for transitions of type (b) arises from the pressure-dependent cascade cross sections from higher levels that are optically coupled to the ground level, like level α. The ob-

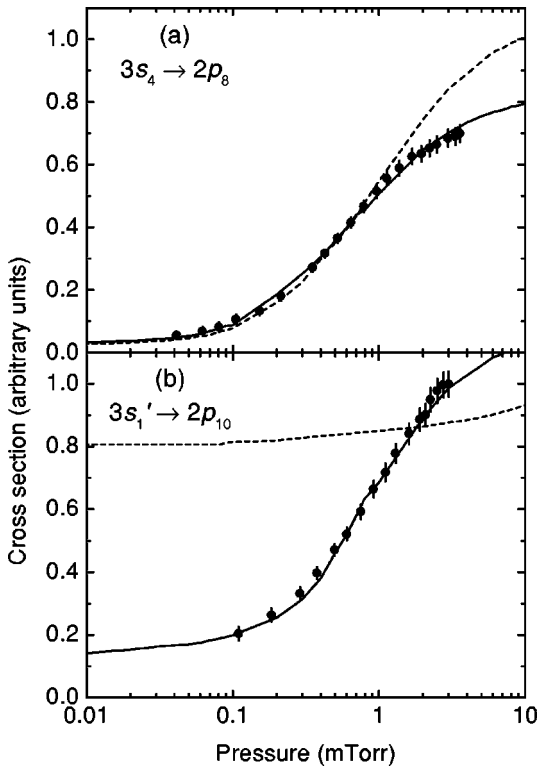

FIG. 3. Cross section versus pressure for transitions out of the (a) $3s_4$ and (b) $3s_1'$ levels of krypton. The dashed line is the result of applying the Heddle radiation trapping model with the theoretical transition probabilities from Ref. [12]. The solid line is a fit to the model with adjusted values of the transition probabilities.

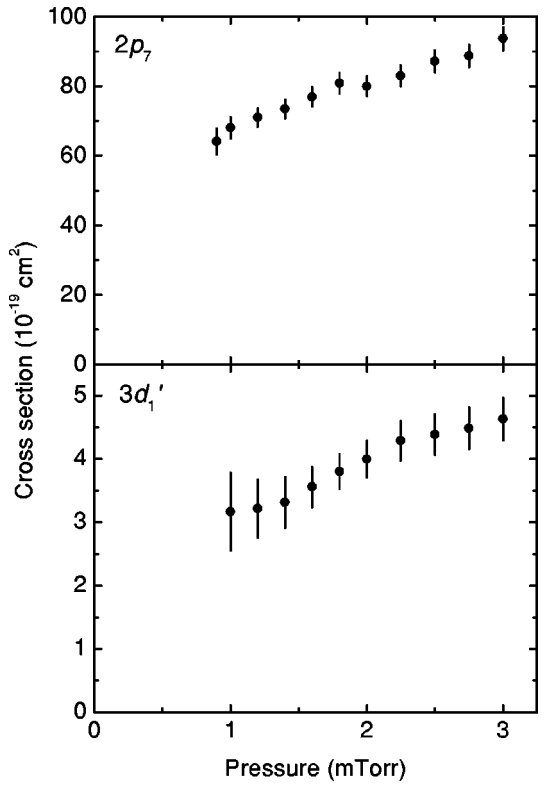

FIG. 4. Apparent excitation cross section versus pressure for two krypton levels not optically coupled to the ground level.

served pressure effects for these two types of transitions are discussed separately in the following paragraphs.

Figure 3 shows the pressure dependence of the optical cross sections for emission from the $3s_4$ level (Paschen's notation for one of the $4p^5 7s$, $J=1$ levels) and the $3s_1'$ level (Paschen's notation for one of the $4p^5 4d$, $J=1$ levels), both of which are optically connected to the ground level. The specific emission lines ($\alpha \rightarrow \beta$) that we study are $3s_4 \rightarrow 2p_8$ and $3s_1' \rightarrow 2p_{10}$. Here $2p_8$ and $2p_{10}$ are Paschen's notation for two of the $4p^5 5p$ levels with $J=2$ and $J=1$, respectively (see Fig. 2). For comparison with the reabsorption mechanism we use Eq. (4) to calculate these cross sections at various pressures. The value of ρ in Eq. (4) is taken as 1.4 cm, which was determined from a detailed analysis of the pressure dependence of the He ($3^1P \rightarrow 2^1S$) emission cross sections measured with the same collision chamber [11]. The shape of the pressure dependence curve as given in Eq. (4) also depends parametrically on A_α' and $A_{\alpha 0}$ with a further implicit dependence on $A_{\alpha 0}$ through k_0. Theoretical calculations of the transition probabilities have been reported by Aymar and Coulombe [12]. Because of the complexity of the atomic structure, the accuracy of the calculated transition probabilities is difficult to assess. We find that analysis of the pressure dependence of the emission cross sections may provide relevant information about the transition probabilities.

At very low pressures, reabsorption is negligible so that $g(k_0\rho)$ approaches unity and Eq. (4) simply restates the well known relation connecting the optical emission cross section to the apparent excitation cross section ($Q_\alpha^{\mathrm{dir}} + Q_\alpha^{\mathrm{casc}}$) and the branching fraction. At the high-pressure limit, $g(k_0\rho)$ tends to zero and the $A_{\alpha 0}$ term in Eq. (4) disappears, corresponding to complete reabsorption of resonant radiation. The ratio of the cross section at these two limits is

$$\frac{Q_{\alpha\beta}^{\mathrm{opt}}(P \rightarrow \infty)}{Q_{\alpha\beta}^{\mathrm{opt}}(P \rightarrow 0)} = 1 + \frac{A_{\alpha 0}}{A_\alpha'}. \tag{5}$$

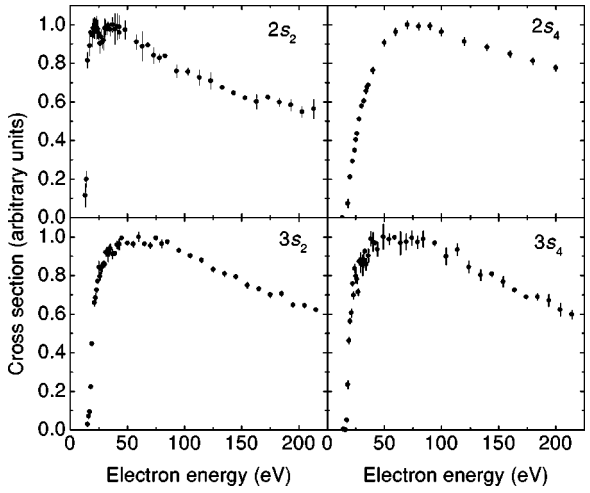

FIG. 5. Apparent excitation functions for the $4p^5 ns$ $J=1$ levels.

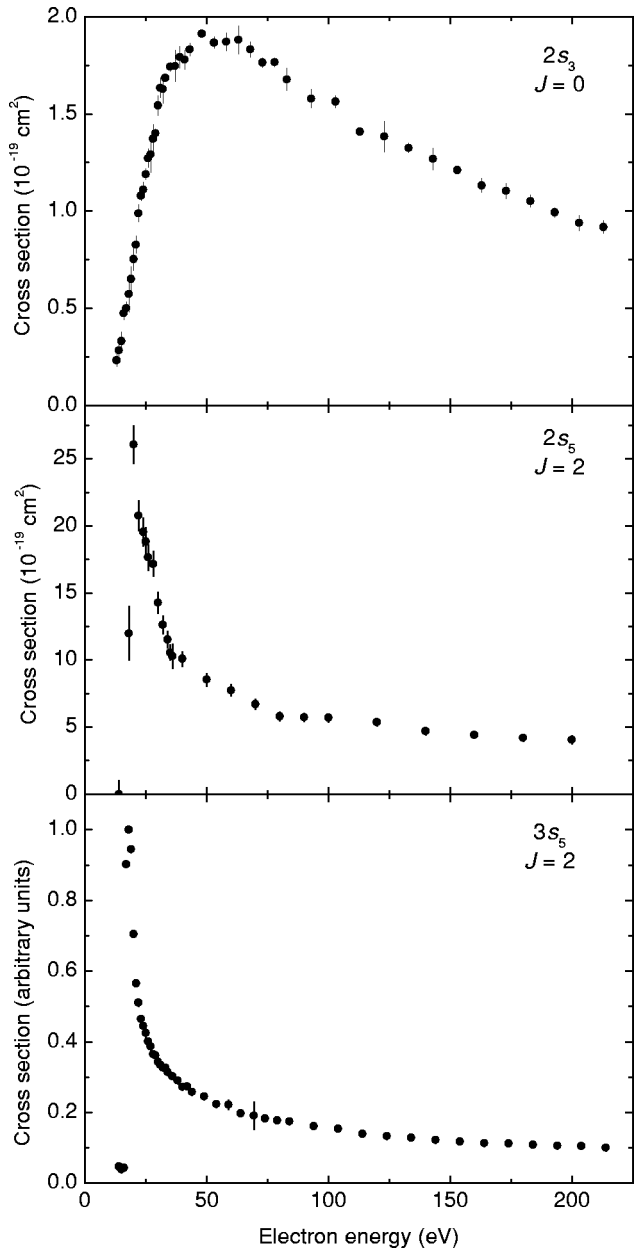

FIG. 6. Apparent excitation functions for the $4p^5ns$ $J\neq 1$ levels.

Thus, the ratio of the measured emission cross sections at the two pressure extremes gives the ratio $A_{\alpha 0}/A'_{\alpha}$. Even if the measurements were not carried to the full asymptotic limits, the pressure dependence of the cross sections can still be used to check the transition probabilities. For instance, from the pressure dependence of the apparent excitation cross section shown in Fig. 3(a), we estimate $Q(P\rightarrow\infty)/Q(P\rightarrow 0)$ for the $3s_4\rightarrow 2p_8$ transition to be about 36, or correspondingly the value $A_{\alpha 0}/A'_{\alpha}\approx 35$. The theoretical values from Ref. [12] are $A_{\alpha 0}=3.0\times 10^8$ s^{-1} and $A'_{\alpha}=5.7\times 10^6$ s^{-1}, yielding $A_{\alpha 0}/A'_{\alpha}=53$, which is considerably larger than our estimate. Indeed, if we adopt these values from Ref. [12] as input to Eq. (4), the calculated pressure dependence overestimates the cross sections at high pressures relative to the low-pressure values. This is demonstrated by the dashed curve in Fig. 3(a). However, by increasing A'_{α} to 8.9×10^6 s^{-1} and keeping $A_{\alpha 0}=3.0\times 10^8$ s^{-1} we obtain a good fit to the measured cross sections as shown in Fig. 3(a). We have also examined the possibility of varying $A_{\alpha 0}$. Since $A_{\alpha 0}$ is related to k_0 in Eq. (4), an increase in $A_{\alpha 0}$ would shift the rising portion of the curve to the low-pressure side. Test calculations show that a satisfactory fit can be retained if $A_{\alpha 0}$ is chosen within the range of 2.4×10^8 to 3.8×10^8 s^{-1}, with a corresponding adjustment of A'_{α}.

Analysis of the pressure dependence of the $3s'_1\rightarrow 2p_{10}$ emission cross section provides a more stringent test of the theoretical transition probabilities. In Fig. 3(b) the measured cross sections have not yet reached the high-pressure limit. Nevertheless, the experimental data clearly indicate that $Q(P\rightarrow\infty)/Q(P\rightarrow 0)$ must be larger than 5, or $A_{\alpha 0}/A'_{\alpha}>4$. From Ref. [12] we get $A_{\alpha 0}=2.1\times 10^6$ s^{-1} and $A'_{\alpha}=8.5\times 10^6$ s^{-1}, yielding an expected ratio of 1.2. Thus, the theoretical value of $A_{\alpha 0}/A'_{\alpha}$ is much too small. Furthermore, if we input these theoretical values of A'_{α} and $A_{\alpha 0}$ into Eq. (4), the resulting $Q^{\rm opt}_{\alpha\beta}(P)$ shown as the dashed curve in Fig. 3(b) increases by only 8% with a fairly uniform slope in the range of 0.1 to 3 mTorr, and the slope becomes much larger at 10 mTorr. This behavior corresponds to a much weaker reabsorption than is exhibited by the experimental data, indicating that the theoretical value of $A_{\alpha 0}$ is much too small. In fact, it is possible to accurately reproduce the experimental data by using the same A'_{α} and increasing $A_{\alpha 0}$ to 7.5×10^7 s^{-1}. This, however, is not to be taken as a proposed revision of $A_{\alpha 0}$, since the fitting process is not unique. The points we want to make are that the calculated $A_{\alpha 0}$ from Ref. [12] is too small, and that the observed pressure dependence of the $3s'_1\rightarrow 2p_{10}$ emission cross section is consistent with the reabsorption model of Gabriel and Heddle [13].

Finally, we address the pressure effects for the levels that are not optically connected to the ground level. Figure 4 shows optical emission cross section versus pressure for a $4p^55p$ level with $J=1$ and a $4p^54d$ level with $J=3$. Neither level is optically coupled to the ground level, yet each show optical emission cross sections that increase with pressure. This variation with pressure is due to the pressure-dependent cascade contribution to the apparent cross sections. The $4p^55p$, $J=1$ level receives cascade from resonant levels. The $4p^54d$, $J=3$ level receives cascade from higher-lying $4p^5np$ levels, which themselves receive resonant cascade subject to radiation trapping. Thus, all optical emission cross sections exhibit some degree of pressure dependence. For nonresonant levels, the pressure effect is solely due to cascade; thus, the pressure dependence of the optical cross sections for emission from the nonresonant levels is generally weaker than that from the resonant levels.

B. Apparent excitation cross sections of the $4p^5ns$ levels

Excitation functions for the $J=1$ levels of the $4p^56s$ and $4p^57s$ configurations ($2s_2$, $2s_4$, $3s_2$, and $3s_4$ in Paschen's notation) are shown in Fig. 5. Note that all have the broad shape characteristic of the optically allowed levels. In Ar and Ne, excitation functions for the corresponding levels are

TABLE I. Cross sections for cascade into the $2p$ levels measured at 2 mTorr and 100 eV in units of 10^{-20} cm^2. Numbers in parentheses were obtained with the aid of the theoretical transition probability ratios of Ref. [12], and agree with the experimental upper limit. Numbers in curly braces denote cross sections obtained with the aid of the theoretical transition probability ratios but not confirmed from the experimental upper limit; e.g., overlapping lines or a line outside the detection region. An ''X'' represents energetically forbidden cascades into the $2p$ levels. Error bars represent statistical uncertainty only. The last four rows list contributions from the $4p^5 7s$ ($3s_2$–$3s_5$), $4p^5 8s$ ($4s_2$–$4s_5$), $4p^5 5d$ ($\Sigma 4d, 4s_1$), and $4p^5 6d$ ($\Sigma 5d, 5s_1$) levels.

	J	$2p_1$ 0	$2p_2$ 2	$2p_3$ 1	$2p_4$ 1	$2p_5$ 0	$2p_6$ 2	$2p_7$ 1	$2p_8$ 2	$2p_9$ 3	$2p_{10}$ 1
$2s_2$	1	(2.2)	26±5	9.5±1.4	11±2	(0)	(0.6)	2.3±0.3	<0.08		<0.02
$2s_3$	0			8.6±3.0	(5)			(0.2)			0.22±0.06
$3s_1'$	1	<1	<12	<15	40±3	<10	4.7±0.5	2.1±0.3	4.6±0.3		31±2
$3s_1'''$	3	<15					(0.1)		{3.5}	3.5±0.4	
$3s_1''''$	2		11±1	<6	<10		<3	<3	<0.3	<0.3	0.80±0.18
$3s_1''$	2		(0.6)	(5)	(0.05)		5.0±0.7	(0.6)	(0.3)	(0.05)	{0.08}
$2s_4$	1	{0}	{0}	{0}	{0}	(14)	(58)	410±25	219±14		98±8
$3d_2$	1	{0}	{0}	{0}	{0}	49±3	(1) [a]	23±4	149±10		18±5
$2s_5$	2		{0}	{0}	{0}		(2.9)	(2.8)	(3)	28±3	24±2
$3d_1'$	3		{0}				26±2		(3)	13±3	
$3d_1''$	2		{0}	{0}	{0}		(0.4)	(15)	11±3	(0.7)	(0.1)
$3d_4$	3	X	{0}				(<0.1)		(59) [b]	(<12)	
$3d_4'$	4	X	X							17±1	
$3d_3$	2	X	X	X	{0}		<8	<5	<3	(0)	(10)[a]
$3d_5$	1	X	X	X	X	<2	<5	23±1	<5		(12)[b]
$3d_6$	0	X	X	X	X			<10			<5
$\Sigma 7s$		2.9±0.6	7.0±1.4	3.0±0.6	11±2	6.0±0.8	46±8	98±14	144±15	0	27±3
$\Sigma 8s$		0	0	0	0	0	6.7±1.1	13±2	24±3	0	1.6±0.3
$\Sigma 5d$		23±4	14±2	14±3	25±5	28±5	6.8±0.9	9.3±1.3	37±4	4.3±0.6	34±6
$\Sigma 6d$		0	0	0	0	3.8±0.6	0.9±0.1	2.5±0.5	5.0±0.8	0	8.0±1.2

[a]For the unresolved pair of lines marked *a* and the pair marked *b*, the theoretical branching ratios do not agree well with the data, leading to large uncertainty in the correct apportionment of this cascade.

found to be often distorted by a large cascade contribution, producing sharp peaks near onset, but this effect is absent in krypton, except for the $2s_2$ level. Emissions from the resonant levels to the ground level are in the far uv, beyond our detection capabilities. Thus, no absolute apparent excitation cross sections are reported.

For the $J \neq 1$ members of the $4p^5 6s$ and $4p^5 7s$ manifolds, the $2s_5$ and $3s_5$ levels both have the characteristic sharply peaked excitation functions expected of triplet levels.

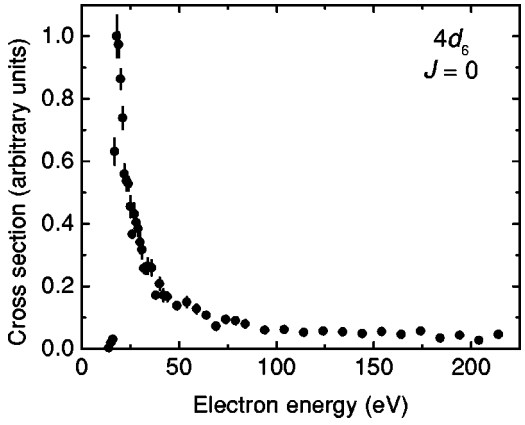

FIG. 7. Apparent excitation functions for the $4d_6$ level.

We measured the emissions from $2s_5$ into the lower $2p$ subgroup, which is optically accessible with our apparatus. Transitions from $2s_5$ into the upper $2p$ subgroup are expected to have very small branching fractions and are neglected because they involve a change of the ion core (from $^2P_{3/2}$ to $^2P_{1/2}$) and have very long wavelengths (5 to 6 μm). The apparent excitation cross sections of the $2s_5$ level are displayed in Fig. 6. As to the $3s_5$ level, transitions into the entire $2p$ set are optically accessible, but transitions into the lower $3p$ subgroup, which do not involve a change of the ion core, are too far in the ir for our detectors. Thus, we do not have the absolute value of the $3s_5$ apparent cross section in Fig. 6. For the ns_3 series, only the $2s_3$ level is given in Ref. [15]. This level, however, exhibits an excitation function that, while still sharper than those for the $J=1$ levels, is significantly broader than the ns_5 levels, in contrast to Ne and Ar for which both the ns_3 and ns_5 levels have sharply peaked excitation functions characteristic of purely triplet levels. The reasons for the anomalous shape of the ns_3 excitation functions are not clear, although various speculations can be offered. It may be due to distortion by cascades. It is also possible that because the ns_3 and ns_2 levels are very close together (Fig. 2), coupling of these two levels through the colliding electron may have important influence on the excitation cross sections, whereas the ns_5 levels are much

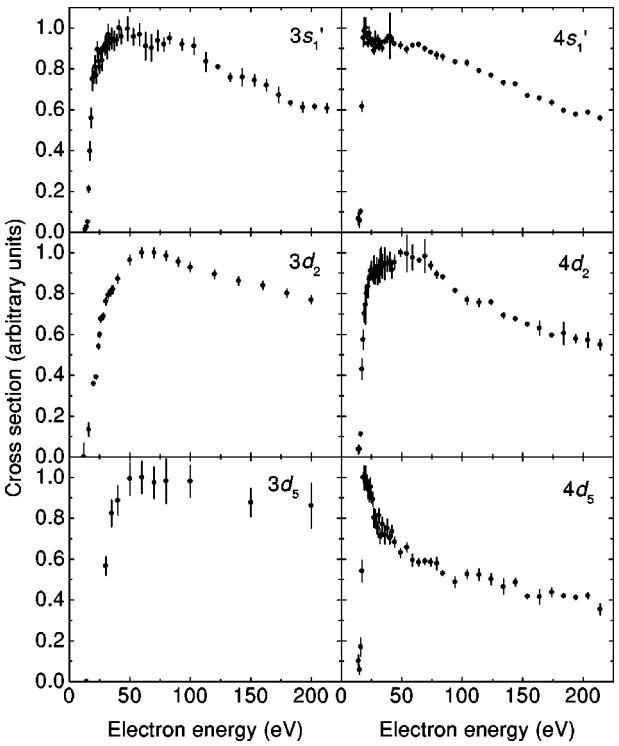

FIG. 8. Apparent excitation functions for the $4p^5nd$ $J=1$ levels.

farther apart from ns_4, and are less susceptible to the coupling via the incident electron. One should also remember that ns_3 is a purely triplet level only under the one-configuration approximation. Mixing of ns_3 with $J=0$ levels from other configurations may result in singlet admixture and therefore broaden the excitation function. Further studies are needed to clarify this point.

Table I gives the optical cross sections for the emission from the $4p^5ns$ levels into the ten $2p$ levels, measured at 2 mTorr and 100 eV. In some cases when the transition $i \rightarrow 2p_a$ is not discernible from the noise level, one can infer its cross section by measuring a different transition $i \rightarrow 2p_b$ and using the ratio of the theoretical transition probabilities for these two transitions. This inferred value is usually consistent with the upper limit that we place on the cross section based on the minimum detectable signal at that wavelength. Cross sections measured indirectly in this manner are annotated in Table I.

C. Apparent excitation cross sections of the $4p^5nd$ levels

Each $4p^5nd$ manifold has two pure triplet levels: d_6 ($J=0$) and d_4' ($J=4$) in Paschen's notation. The two optically allowed transitions from the $3d_6$ level are in the ir region where our InSb detector has low sensitivity, and were not found in our experiment. The excitation functions for the $3d_4'$ transitions exhibit poor signal-to-noise ratios, although they are consistent with the expected sharply peaked shapes. Transitions from the $4d$ levels occur in the more favorable part of the spectrum. Unfortunately, the $4d_4'$ level emits at the same wavelength as the much stronger $2p_8 \rightarrow 1s_5$ transi-

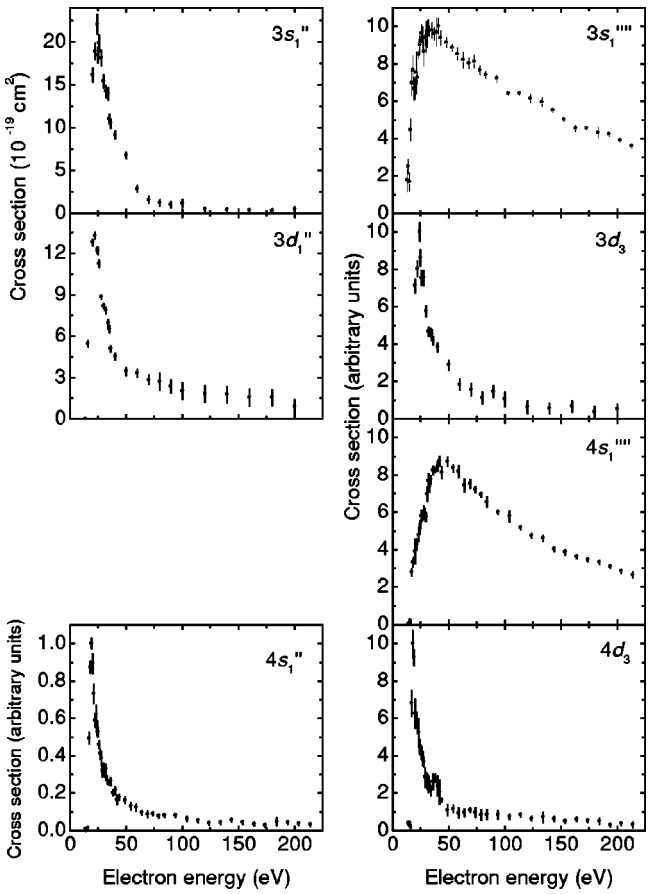

FIG. 9. Apparent excitation functions for the $4p^5nd$ $J=2$ levels.

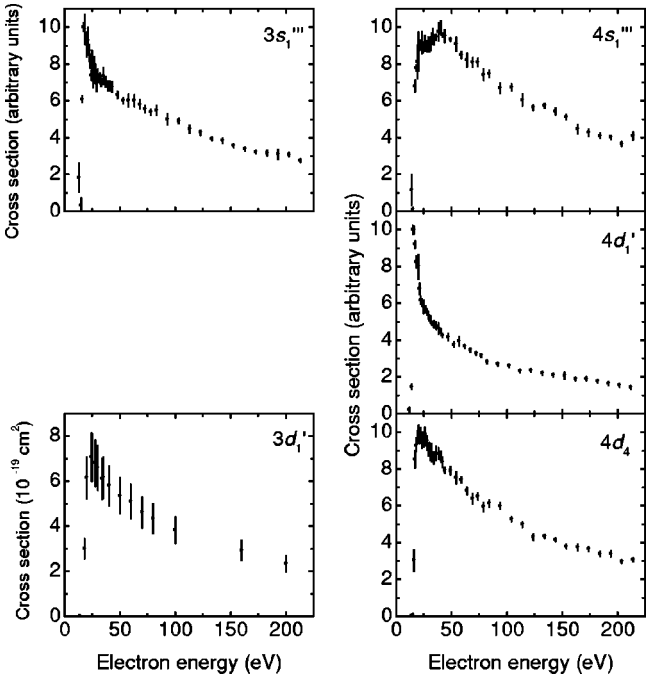

FIG. 10. Apparent excitation functions for the $4p^5nd$ $J=3$ levels.

TABLE II. Optical emission cross sections for the $2p \rightarrow 1s$ emissions of Kr at 100 eV in units of 10^{-19} cm^2. The individual emission cross sections are given at 2 mTorr. Values in brackets were obtained using theoretical values of the branching ratios. The last row lists apparent cross sections at low pressure (below 0.1 mTorr), where pressure effects are no longer important. Emissions from the $2p_{10}$ level could not be observed at this low pressure.

		$2p_1$	$2p_2$	$2p_3$	$2p_4$	$2p_5$	$2p_6$	$2p_7$	$2p_8$	$2p_9$	$2p_{10}$
	J	0	2	1	1	0	2	1	2	3	1
$1s_2$	1	20	24	3.8	8.1	[0]	[0.1]	[0.1]	[0.1]		[0.03]
$1s_3$	0			5.0	6.3			[0.07]			[0.06]
$1s_4$	1	0.030	1.0	0.036	0.18	47	9.4	69	63		3.3
$1s_5$	2		0.14	0.76	0.17		28	11	32	19	28
Sum ($P=2$)		20 ± 2	25 ± 3	10 ± 1	15 ± 2	47 ± 6	37 ± 4	80 ± 10	95 ± 12	19 ± 3	31 ± 6
Sum ($P=0.1$)		18 ± 2	23 ± 4	5.8 ± 2.6	6.6 ± 2.1	42 ± 6	30 ± 3	43 ± 7	49 ± 6	14 ± 3	

tion, so that we cannot make the measurement. Only the $4d_6$ level is accessible and its cross section, shown in Fig. 7, has the usual sharp peak characteristic of triplet levels.

The $J=1$ members of the $4p^5 4d$ ($3s_1'$, $3d_2$, and $3d_5$ in Paschen's notation) and $4p^5 5d$ ($4s_1'$, $4d_2$, and $4d_5$) manifolds are shown in Fig. 8. All excitation functions have very broad shapes, characteristic of levels optically coupled to the ground. We note, however, that the $4s_1'$ and especially the $4d_5$ levels show pronounced peaks near onset, indicating a possible large cascade component.

Results for the $J=2$ levels are displayed in Fig. 9. No transitions from the $4d_1''$ level were detected. All levels except $3s_1'''$ and $4s_1'''$ show very narrow excitation functions expected of levels with no direct Coulomb coupling to the ground level through the colliding electron. The broad shapes of the two exceptions, which differ greatly from the other levels in this family, are reminiscent of the anomalous case of the $2s_3$ level discussed in Sec. III B. Such deviations from the general rules may point toward some especially interesting features for Kr.

Finally, the cross sections for the $J=3$ levels are shown in Fig. 10. These levels exhibit excitation functions that are somewhat broader in shape than for the very sharp functions of the $J=2$ levels, because, unlike the case of $J=2$, the $J=3$ levels do couple with the ground level through the Coulomb interaction with the colliding electron. On the other hand, the $J=3$ levels are not optically connected to the ground level; hence we find narrower excitation functions than for the $J=1$ levels. The only transition from $3d_4$ that is strong enough to detect is $3d_4 \rightarrow 2p_8$, which is not completely resolved from the $3d_5 \rightarrow 2p_{10}$ line (only 2 cm^{-1} apart). Thus, no $3d_4$ data are included in Fig. 10.

Note that in the figures not all excitation functions have been placed on an absolute scale. Those displayed on absolute scales indicate that all transitions out of the level have been measured. Those on arbitrary scales indicate that not all transitions out of the level could be measured, either because of difficulty in separately identifying multiple transitions with very close wavelengths, or due to transitions falling outside the detection range of the experiments. Absolute values of the optical cross sections for the transitions from the $4p^5 nd$ levels into the ten $2p$ levels measured at 2 mTorr and 100 eV are given in Table I.

D. Direct excitation cross sections of the $4p^5 5p$ levels

The majority of transitions out of the $4p^5 5p$ manifold lie in the visible spectral region and are easily measured. The transitions from the lower subgroup of $4p^5 5p$ to the upper subgroup of $4p^5 5s$ lie in the ir, accessible with our detector system. None of these transitions were observed, however, due to the unfavorable line strengths for transitions involving a change from the $^2P_{3/2}$ ion core into the $^2P_{1/2}$ core. Their values have thus been estimated with theoretical branching ratios, and constitute no more than 0.3% of the apparent excitation cross sections. Transitions from the $4p^5 5p$ to $4p^5 4d$ levels are all in the far-ir region, outside our detector range, but are negligible, as explained in the beginning of Sec. III. Table II lists values for optical emission cross sections out of the $4p^5 5p$ levels at 100 eV and 2 mTorr pressure. Due to the radiation trapping mechanism discussed in Sec. III A, these emission cross sections vary with pressure. Thus, apparent cross sections in Table II are given at 2 mTorr and also at a low pressure (generally below 0.1 mTorr), where the cross sections become constant with pressure.

By subtracting the cascade contributions (Secs. III B and III C and Table I) from the apparent $4p^5 5p$ cross sections, it is possible to determine direct electron excitation cross sections for these levels. Because of the pressure dependence of the emission cross sections, it is important that the cascade and apparent cross sections are measured at the same pressure. Figure 11 shows the results. For the two $J=0$ levels, $2p_1$ and $2p_5$, the cascade originates entirely from the resonant $J=1$ levels. The very broad peak associated with these cascading resonant levels is responsible for the secondary maxima evident in the apparent excitation functions. For the four $J=1$ levels, the effect of the cascade is to broaden the high-energy section of the apparent excitation functions. Note particularly the effect on $2p_7$, where the cascade cross section is significantly larger than the direct excitation cross section beyond about 50 eV. Finally, consider the three $J=2$ and the one $J=3$ levels. Only for $2p_8$ does the cascade

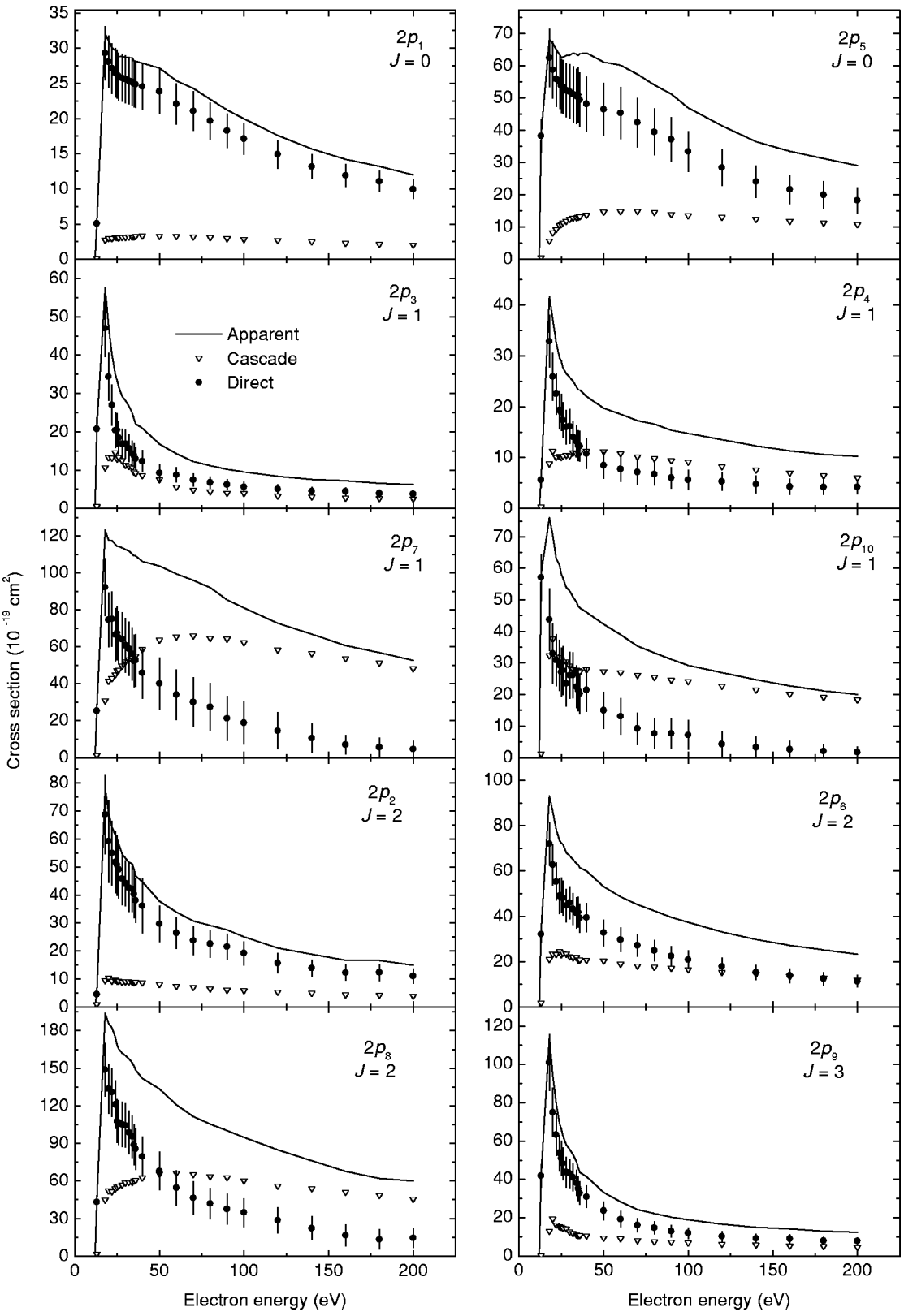

FIG. 11. Apparent (line), cascade (triangles), and direct (circles) cross sections for the $4p^5 5p$ levels.

surpass the direct cross section.

As in the case of neon and argon, the $2p_9$ level exhibits a narrow-peak excitation function characteristic of a purely triplet state. The $J=1$ excitation functions are only slightly broader than the $2p_9$ function, and are narrower than those of the $J=2$ and $J=0$ levels. This can be understood by considering that the Coulomb potential of the incident electron does not couple these $J=1$ levels with the ground level,

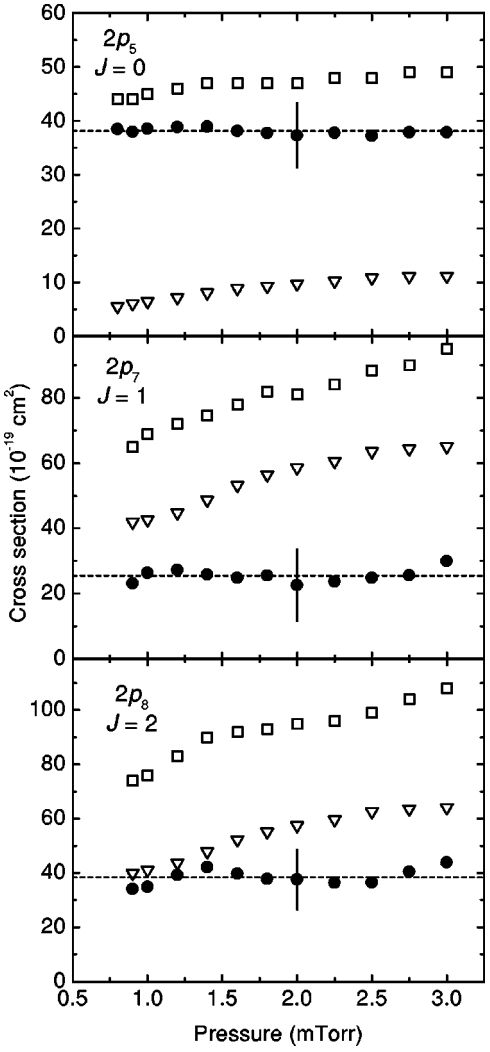

FIG. 12. Apparent (squares), cascade (triangles), and direct (circles) cross sections at 100 eV versus pressure for three of the $4p^55p$ levels. The dashed horizontal line represents the average direct cross section.

so that excitation must proceed through indirect coupling via intermediate states or exchange interaction. On the other hand, there exists direct Coulomb coupling between the even-J levels with the ground, which manifests itself most clearly in the broad shape of the direct excitation functions of the $J=0$ levels.

The data in Figure 11 were all acquired at a target gas pressure of 2 mTorr. To study the pressure effects, we have repeated the cascade and apparent measurements across the 0.8–3 mTorr range, and determined the direct cross sections at different pressures. The result, shown in Fig. 12, is that, while both the apparent and cascade cross sections increase with pressure, the direct cross sections, within error bars, remain constant. This indicates that the pressure dependence of the cascade cross sections, which we attribute to resonance radiation reabsorption, is entirely responsible for the pressure dependence of the apparent cross sections.

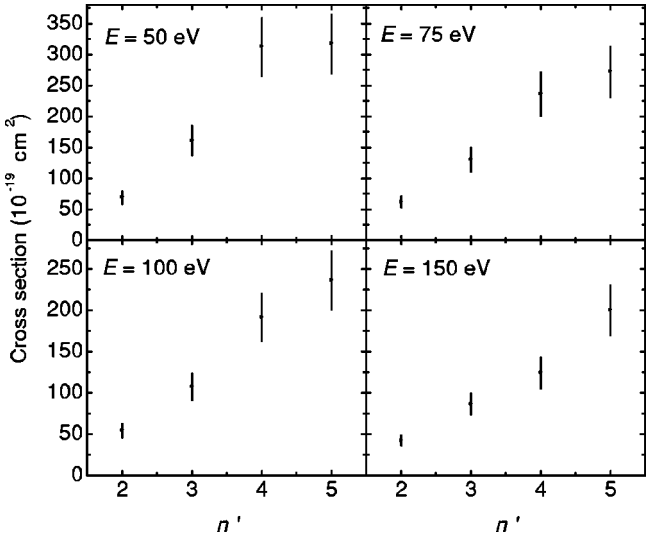

FIG. 13. Direct excitation cross sections for excitation into the entire $n'p^5(n'+1)p$ manifold versus n' for Ne, Ar, Kr, and Xe.

E. Magnitudes of the cross sections and comparison with Ne, Ar, and Xe

It was stated earlier that the direct excitation cross sections for the levels within a given configuration like $2p^5nl$ or $3p^5nl$ for neon and argon obey a parity rule whereby levels with $J+l$ odd tend to have larger cross sections than those with $J+l$ even. In the case of xenon, our analysis must be modified by dividing a configuration into two subgroups corresponding to the $^2P_{3/2}$ and $^2P_{1/2}$ ion cores. The levels with the $^2P_{3/2}$ ion core generally have larger cross sections than the levels with the $^2P_{1/2}$ core; however, within each subgroup, the $(J+l)$ parity rule similar to neon and argon holds. Now that we have direct cross sections for the $4p^55p$ levels, we can examine trends in the direct cross sections for krypton.

Table III gives direct electron excitation cross sections at various energies for the ten levels of the Kr $4p^55p$ configuration, listed in the order of the two subgroups with the $^2P_{1/2}$ ion core ($2p_1$ through $2p_4$) and the $^2P_{3/2}$ core ($2p_5$ through $2p_{10}$). At an incident energy of 75 eV and above, within each group the even-J levels have larger cross sections than the odd-J levels, conforming to the $(J+l)$ rule with $l=1$. In fact, this parity relation holds even at 30 eV with only one exception. Next we compare the two subgroups with each other. The lower subgroup (the $^2P_{3/2}$ core) as a whole does have larger cross sections than the upper subgroup (the $^2P_{1/2}$ core) with roughly a factor of 2 in the average cross section. However, individually some of the odd-J levels of the lower subgroup have smaller cross sections than the even-J levels of the upper subgroup. This is because the odd-J levels inherently have smaller cross sections than the even-J levels of the same subgroup. Indeed, if we limit our comparison to either even-J only or odd-J only, then the lower subgroup clearly has larger cross sections than the upper subgroup.

The foregoing discussions indicate that the magnitudes of the cross sections are influenced by two criteria. The first one

TABLE III. Direct electron excitation cross sections for the $4p^5 5p$ levels of Kr in units of 10^{-19} cm^2. Error bars represent combined statistical and systematic errors. Cross sections peak near 18 eV.

	J	Peak	30 eV	50 eV	75 eV	100 eV	200 eV
$2p_1$	0	29±4	26±3	24±3	20±3	17±2	10±1
$2p_2$	2	69±14	44±11	30±6	23±5	19±4	11±3
$2p_3$	1	47±7	17±4	9.3±2.2	7.2±1.5	5.6±1.3	3.8±0.8
$2p_4$	1	33±5	16±3	8.5±2.6	7.0±2.2	5.6±1.9	4.2±1.3
$2p_5$	0	62±9	51±8	47±8	41±7	34±6	18±4
$2p_6$	2	72±10	46±7	33±6	26±5	21±4	11±3
$2p_8$	2	149±21	104±17	68±15	45±13	35±11	15±7
$2p_7$	1	93±15	61±15	40±14	29±13	19±11	4.6±5.2
$2p_{10}$	1	57±7	27±7	15±6	8.5±4.8	7.2±4.6	1.7±2.3
$2p_9$	3	101±14	43±7	24±5	16±3	12±3	7.9±1.8

is the $(J+l)$ parity rule, which, for the case for the $n'p^5np$ configuration of rare gases ($n'=2,3,4$, and 5 for Ne, Ar, Kr, and Xe, respectively), favors excitation into the levels with even J (odd values of $J+l$) over those with odd J (even values of $J+l$) at high energies. The second criterion is that when two levels within a configuration have substantially different ionization energies, excitation tends to favor the lower level. Unlike the first criterion, the second criterion is not limited to high energies. For the lower excited configurations of neon and argon, all the levels within the same configuration have nearly the same ionization energy. Thus, the second criterion has no effect and the parity rule prevails for all the levels in a configuration. In the other extreme is xenon, for which the $5p^5 6p$ configuration consists of two subgroups of very different ionization energies (1.1 and 2.4 eV), resulting in two correspondingly distinct sets of cross sections. Krypton proves to be an intermediate case. The $4p^5 5p$ levels still segregate into two subgroups with about 40% difference in ionization energy. Thus, both the first and second criteria apply so that the even-J levels of the lower subgroup are the most favorable ones for excitation whereas the odd-J levels of the upper subgroup are the least favorable. The odd-J levels of the lower subgroup and the even-J levels of the upper subgroup are favored by one criterion but disfavored by the other; hence, their cross sections overlap. The more complex behaviors of krypton can therefore be understood as an intermediate case of a unified picture for the entire rare-gas series.

F. Comparison of the $n'p \rightarrow (n'+1)p$ cross sections for the rare gases

The sum of the cross sections of all ten $2p$ levels represents the excitation from the $n'p^6$ ground state into the entire $n'p^5(n'+1)p$ manifold, and therefore corresponds to the $n'p \rightarrow (n'+1)p$ excitation, with $n'=2,3,4$, and 5 for Ne, Ar, Kr, and Xe respectively. In Fig. 13 we plot these manifold cross sections $Q[n'p^5(n'+1)p]$ versus n' for the four rare-gas atoms at 50, 75, 100, and 150 eV. The nearly linear relationship at 75, 100, and 150 eV is interesting. Here the cross section increases by roughly a factor of 2 from Ne to Ar, a factor of 3 from Ne to Kr, and a factor of 4 from Ne to Xe. Let us compare these increases with the ''size'' of the atoms. Different sets of atomic radii for the rare gases have been derived based on different criteria, but their ratios show much less variance. From Ref. [16] we take the atomic radii ratio as 1.2 for Ne to Ar, 1.3 for Ne to Kr, and 1.4 for Ne to Xe. Thus, the increments in the manifold cross sections are

TABLE IV. Comparison of our cross section results with the experimental results of [21] and the theoretical results of [23] for the $4p^5 5p$ levels in units of 10^{-19} cm^2. Error bars in our data represent combined statistical and systematic errors. Cross sections peak near 18 eV.

	J	This work peak	Ref. [21] expt. peak	Ref. [23] theory peak	This work 100 eV	Ref. [21] expt. 100 eV	Ref. [23] theory 100 eV
$2p_1$	0	29±4	26±9		17±2	20±7	
$2p_2$	2	69±14	55±19	29	19±4	22±8	24
$2p_3$	1	47±7	18±6	4.0	5.6±1.3	4.4±2.2	0.025
$2p_4$	1	33±5	24±8	16	5.6±1.9	2.4±1.2	0.067
$2p_5$	0	62±9	31±11		34±6	25±9	
$2p_6$	2	72±10	17±6	24	21±4	9.9±3.5	9.9
$2p_7$	1	93±15	24±8	11	19±11	15±5	0.052
$2p_8$	2	149±21	81±28	43	35±11	49±17	35
$2p_9$	3	101±14	35±12	35	12±3	3.1±1.6	0.16
$2p_{10}$	1	57±7		25	7.2±4.6		0.067

much larger than what may be expected of the geometric size. We may also contrast this trend with the $n's \rightarrow n'p$ excitation of the alkali-metal atoms. At 50 eV the direct excitation cross sections for Li ($2s \rightarrow 2p$), Na ($3s \rightarrow 3p$), and K ($4s \rightarrow 4p$) are 2.0×10^{-15}, 2.2×10^{-15}, and 2.9×10^{-15} cm^2 [17–19], a much milder increase than for the rare gases. Of course, excitation cross sections depend on both the initial (ground) state and the final state, whereas the atomic radius is a ground-state property. A quantitative understanding of the trend of large increase in Fig. 13 should be valuable toward a comprehensive insight into the excitation processes of the rare-gas series.

G. Comparison with other experiments and theory

Fel'tsan [20] reported measurements of the optical emission cross sections for transitions of the type $4p^5 5p \rightarrow 4p^5 5s$ in the pressure region of 1–5 mTorr. Cross sections for only a few transitions into the $4p^5 5p$ levels were measured; thus, the direct excitation cross sections were not determined. Since the exact pressures at which his data were taken are not given, quantitative comparison of his cross sections with ours is not possible because of the pressure dependence of the optical emission cross sections. Fel'tsan found a double-peak structure for the excitation functions of the $2p_1$, $2p_5$, and $2p_7$ levels which we also observe, although his double-peak structure is more prominent than ours.

Bogdanova and Yurgenson [21] have used a pulsed electron beam to measure the excitation cross sections of the $4p^5 5p$ levels of krypton, attempting to eliminate the cascade contribution. Table IV compares their measurements with the present work. At peak cross section, the agreement for the upper subgroup is quite good. For the lower subgroup, however, our results are larger than those of Ref. [18]. At 100 eV, the agreement between the two experiments is generally better.

Trajmar *et al.* [22] have measured inelastic differential cross sections (DCS's) for excitation of Kr atoms into a number of higher levels. The individual higher levels were not completely resolved, but cross sections were reported for various ''features'' which correspond to one or more excited levels. The integral cross sections obtained by integrating the DCS over the scattering angle may be compared with our direct excitation cross sections. In Ref. [22], excitation into the $4p^5 5p$ levels that are isolated from other configurations include features 5 ($2p_{10}$); 6 ($2p_9+2p_8$); 7,8 ($2p_7+2p_6$); and 9 ($2p_5$). Their integral cross sections at 30 eV are 7.2, 49, 25, and 29 in units of 10^{-19} cm^2, respectively; considerably smaller than the corresponding values of 27, 147, 107, and 51 from our measurements.

The only theoretical work on the excitation cross sections of krypton that we are aware of is by Kaur *et al.* [23], using a relativistic distorted wave method. They published results using both single-configuration and multiconfiguration ground-state wave functions. Their multiconfiguration results are also included in Table IV. No clear trend is apparent on comparing their theoretical results to experiment, although their calculations are generally smaller than the measured cross sections.

IV. CONCLUDING REMARKS

Our experiments reported here not only provide the electron-impact excitation cross section data for Kr, but also allow us to compare the results for the four rare gases. In particular, we examine the excitation from the $n'p^6$ ground state into the ten levels in the $n'p^5(n'+1)p$ configuration with $n'=2,3,4,$ and 5 for Ne, Ar, Kr, and Xe. The variations of the cross sections for the different levels can be explained by consideration of the ionization energy and the parity of the J value. Another point of interest is that the cross section for excitation into the entire $n'p^5(n'+1)p$ manifold for the rare gases increases quite drastically from Ne to Xe; much more than expected from consideration of the atomic size.

Apparent excitation cross sections have been measured for the levels in the $4p^5 6s$, $4p^5 7s$, $4p^5 3d$, and $4p^5 4d$ configurations of Kr. The shape of the excitation functions for the various levels can be classified according to the value of J as was done for the other rare-gas atoms. However, an important exception was found for the $J=0$ level of the $4p^5 6s$ configuration. The reason for this exception is not understood, and it merits further studies.

ACKNOWLEDGMENT

This work was supported by the Air Force Office of Scientific Research.

[1] J. E. Chilton, J. B. Boffard, R. S. Schappe, and C. C. Lin, Phys. Rev. A **57**, 267 (1998).
[2] J. E. Chilton and C. C. Lin, Phys. Rev. A **60**, 3712 (1999).
[3] F. A. Sharpton, R. M. St. John, C. C. Lin, and F. E. Fajen, Phys. Rev. A **2**, 1305 (1970).
[4] J. E. Chilton, M. D. Stewart, Jr., and C. C. Lin, Phys. Rev. A **61**, 052708 (2000).
[5] J. T. Fons and C. C. Lin, Phys. Rev. A **58**, 4603 (1998).
[6] M. L. Bhaumik, R. S. Bradford, Jr., and E. R. Ault, Appl. Phys. Lett. **28**, 23 (1976).
[7] M. V. Malyshev, V. M. Donnelly, and S. Samukawa, J. Appl. Phys. **84**, 1222 (1998).
[8] M. V. Malyshev and V. M. Donnelly, Phys. Rev. E **60**, 6016 (1999).
[9] G. G. Lister, in *Advanced Technologies Based on Wave and Beam Generated Plasmas*, edited by H. Schlüter and A. Shivarova (Kluver Academic Publishers, Boston, 1999), p. 65.
[10] A. R. Filippelli, C. C. Lin, L. W. Anderson, and J. W. McConkey, Adv. At., Mol., Opt. Phys. **33**, 1 (1994).
[11] J. E. Chilton and C. C. Lin, Phys. Rev. A **58**, 4572 (1998).
[12] M. Aymar and M. Coulombe, At. Data Nucl. Data Tables **21**, 537 (1978).
[13] A. H. Gabriel and D. W. O. Heddle, Proc. R. Soc. London, Ser. A **258**, 124 (1960).

[14] D. W. O. Heddle and M. J. Samuel, J. Phys. B **3**, 1593 (1970).
[15] C. E. Moore, *Atomic Energy Levels*, Natl. Bur. Stand. (U.S.) Circ. No. 467 (U.S. Government Printing Office, Washington, D.C., 1952), Vol. II.
[16] H. Haken and H. C. Wolf, *Atomic and Quantum Physics*, translated by W. D. Brewer (Springer-Verlag, New York, 1987).
[17] D. Leep and A. Gallagher, Phys. Rev. A **10**, 1082 (1974).
[18] J. O. Phelps and C. C. Lin, Phys. Rev. A **24**, 1299 (1981).
[19] J. O. Phelps, J. E. Solomon, D. F. Korff, C. C. Lin, and E. T. P. Lee, Phys. Rev. A **20**, 1418 (1979).
[20] P. V. Fel'tsan, Ukr. Fiz. Zh. **12**, 1425 (1967) [Ukr. Phys. J. **12**, 1376 (1967)].
[21] I. P. Bogdanova and S. V. Yurgenson, Opt. Spektrosk. **62**, 713 (1987) [Opt. Spectrosc. **62**, 424 (1987)].
[22] S. Trajmar, S. K. Srivastava, H. Tanaka, H. Nishimura, and D. C. Cartwright, Phys. Rev. A **23**, 2167 (1981).
[23] S. Kaur, R. Srivastava, R. P. McEachran, and A. D. Stauffer, J. Phys. B **31**, 4833 (1998).